Alistair A. Young, PhD
Brett R. Cowan, BE, MBChB
Steven F. Thrupp, MA
Warren J. Hedley, ME
Louis J. Dell'Italia, MD

Index terms:
Heart, volume, 51.92
Magnetic resonance (MR), phase imaging, 51.12144
Magnetic resonance (MR), rapid imaging, 51.121416
Magnetic resonance (MR), volume measurement, 51.12144

Radiology 2000; 216:597–602

Abbreviations:
ED = end-diastolic
ES = end-systolic
LV = left ventricle
3D = three-dimensional

[1] From the Departments of Anatomy with Radiology (A.A.Y.), Medicine (B.R.C., S.F.T.), and Engineering Science (W.J.H.), University of Auckland, 85 Park Road, Auckland, New Zealand; and the Department of Medicine, University of Alabama at Birmingham, Ala (L.J.D.). Received August 13, 1999; revision requested October 5; revision received November 12; accepted December 20. Supported in part by the Auckland Medical Research Foundation and the Health Research Council of New Zealand. **Address correspondence to** A.A.Y. (e-mail: *a.young@auckland.ac.nz*).

Author contributions:
Guarantor of integrity of entire study, A.A.Y.; study concepts, A.A.Y., B.R.C.; study design, A.A.Y.; definition of intellectual content, A.A.Y., B.R.C.; literature research, A.A.Y.; clinical studies, B.R.C., L.J.D.; experimental studies, A.A.Y., S.F.T., B.R.C., L.J.D.; data acquisition, A.A.Y., S.F.T., B.R.C., L.J.D.; data analysis, A.A.Y., S.F.T., W.J.H.; statistical analysis, A.A.Y.; manuscript preparation, A.A.Y.; manuscript editing and review, A.A.Y., S.F.T., W.J.H., B.R.C.

Left Ventricular Mass and Volume: Fast Calculation with Guide-Point Modeling on MR Images[1]

The authors describe a fast method for calculating left ventricle (LV) mass and volumes from multiplanar magnetic resonance (MR) images. Mathematic models were fitted to a small number of user-selected guide points in 15 healthy volunteers, 13 patients after myocardial infarction, and a canine model of mitral regurgitation in eight dogs. Errors between model and manual contours were small (LV mass, 1.8 g ± 4.9 [mean ± SD]; end-diastolic volume, 2.2 mL ± 4.6; end-systolic volume, 2.3 mL ± 3.8). Estimates of global function could be obtained in 6 minutes, a time saving of 5–10 times over estimates with manual contouring.

Left ventricle (LV) mass and volumes at end-diastole (ED) and end-systole (ES) are essential clinical parameters for the diagnosis and management of cardiac disease. Magnetic resonance (MR) imaging is able to provide accurate and precise estimations of LV mass and volume since it is a true three-dimensional (3D) method that is not dependent on geometric assumptions and is not limited in the position or orientation of the image sections (unlike echocardiography or computed tomography [CT]) (1,2). Current imaging techniques allow the acquisition of 10–20 sections in short- and long-axis orientations, each with 10–20 frames through the cardiac cycle, in clinically acceptable times (<15 minutes) (3,4). Typically, LV boundaries (contours) are drawn on each section of a series of short-axis images and the outlined areas converted to volumes and summed to produce estimates of volume and mass. Previous studies have shown that this technique gives more accurate and reproducible estimates of volume and mass than do other imaging modalities (2,5–7).

A major limitation of the MR imaging section summation method is the prohibitive time necessary to outline the inner and outer boundaries of the LV in each section at ED and ES. This image contouring bottleneck precludes the use of multiplanar MR imaging in routine clinical care and limits its application to small research trials. Many semiautomated image segmentation algorithms have been applied to this problem (8–10), but these algorithms are not sufficiently robust for routine clinical use. Image pixel intensities are insufficient to adequately constrain the segmentation problem, owing to the limited temporal and spatial resolution, presence of image artifacts, and lack of contrast between blood and muscle. The endocardial trabeculae and papillary muscles also make the inner boundary difficult to define. At present, the amount of time spent on manual editing and correction renders automated methods almost as slow as manual contouring in clinical practice.

In this study, we evaluated a fast, accurate method of calculating LV mass and volumes from multiple MR sections, without the need for image contouring. The method relies on an accurate mathematic model of the LV that is fitted to a relatively small number of data points (guide points) provided by the user. No image processing is required and the method is therefore independent of image quality.

Materials and Methods

Data Acquisition

To determine the accuracy and efficiency of this method, we analyzed results in 15 healthy volunteers and 13 patients with regional abnormalities in wall motion due to myocardial infarction. In-

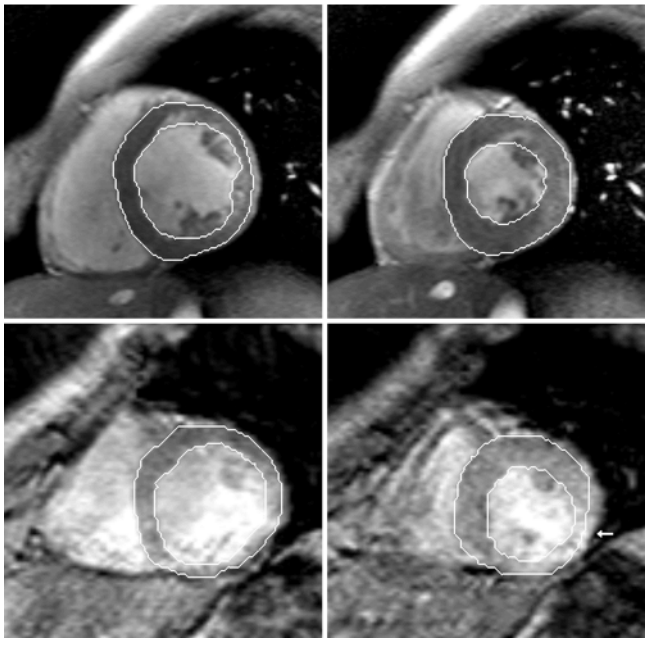

Figure 1. ED (left) and ES (right) gradient-echo short-axis images with manual contours shown as lines. Top: Volunteer images (8/5 with 10° flip angle). Bottom: Patient images (30/14 with 40° flip angle). Note the wall motion abnormality (lack of motion and wall thickening) in the basal lateral wall on the patient image (arrow).

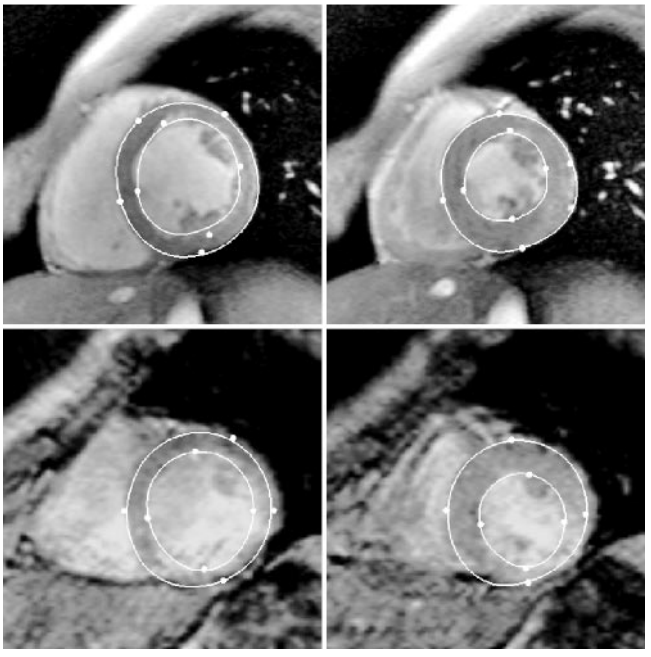

Figure 2. Same images as in Figure 1 with model contours shown as light lines to indicate results of guide-point (●) fit.

formed consent was obtained for all human studies, which were performed with the approval of the institutional ethical committees.

Volunteers.—A group of 15 healthy subjects (10 men and five women; mean age, 23 years; age range, 18–32 years) underwent MR imaging with a 1.5-T imager (Vision; Siemens, Erlangen, Germany). Prospectively gated cardiac cine images were acquired in eight to nine short-axis sections and three long-axis sections with use of a segmented k-space pulse sequence (repetition time msec/echo time msec of 8/5, flip angle of 10°, field of view of 280–350 mm) with view sharing (11–19 frames per section) (3,4). Each section was acquired during a breath hold of 15–19 cardiac cycles. The short-axis sections spanned the heart from apex to base with a section thickness of 8.0 mm and section gap of 0.0–3.0 mm.

Phase-contrast velocity images (11) were acquired in a section positioned perpendicular to the ascending aorta approximately 20 mm above the aortic valve. Since the entire imaging protocol performed with the volunteers consisted of several hours of imaging (including tagging and many flow-quantification sequences), all subjects had a break of 1–2 hours between cine anatomic imaging (including the short-axis cine sections used in the volume calculations) and the phase-contrast flow imaging. At the latter, prospectively gated cine gradient-echo imaging was performed (24/6, flip angle of 30°, field of view of 250 mm, section thickness of 8.0 mm, velocity encoding of 150 or 250 cm/sec, and 25–45 frames through the cardiac cycle). Velocity sensitization was encoded in the through-plane (section-select) direction.

Patients.—MR imaging data from 13 patients, who underwent MR imaging as part of a previous study (12) at 2 weeks ($n = 6$) and 3 months ($n = 7$) after their first acute Q wave myocardial infarction, were selected for analysis of global function. The 13 studies were selected consecutively in alphabetical order from a database of 70 studies, details of which are given by Johnson et al (12). All MR studies were performed with a 1.5-T imager (Gyroscan; Philips, Shelton, Conn). Respiration-compensated gradient-echo cine images (30/14, flip angle of 40°, field of view of 300–400 mm) were acquired in nine to 10 short-axis sections, each 8.0-mm thick with a 1.0-mm section gap.

Animal studies.—MR data from eight dogs imaged 5–6 months after induction of mitral regurgitation, as part of a previous study (13) approved by the institutional animal care committee, were analyzed by means of guide-point modeling. Mitral regurgitation was induced by means of percutaneous chordal rupture of the mitral valvular apparatus, as described in reference 13. MR imaging was performed with a 1.5-T imager (Gyroscan) with the same gradient-echo cine imaging sequences as were used with the patients (six to eight short-axis sections, 8-mm-thick sections, 1.6–4.0 section gap, field of view of 350 mm). After imaging, the hearts were arrested with KCl and removed from the chest. After the atria and right ventricular free wall were removed from the interventricular septum and LV, the portions were weighed.

Image Analysis

Manual contouring and section summation.—The inner and outer boundaries of the LV were defined on each image as follows. First, a semiautomatic region-growing method was used to locate preliminary boundaries (10). These boundaries were then manually corrected for each image. To the best ability of the observer (S.F.T.), papillary muscles were excluded from the myocardium and included in the blood pool. Great care was taken to identify the exact boundary of the myocardium. The contours were then reviewed by another observer (B.R.C.), and a consensus was achieved in all cases

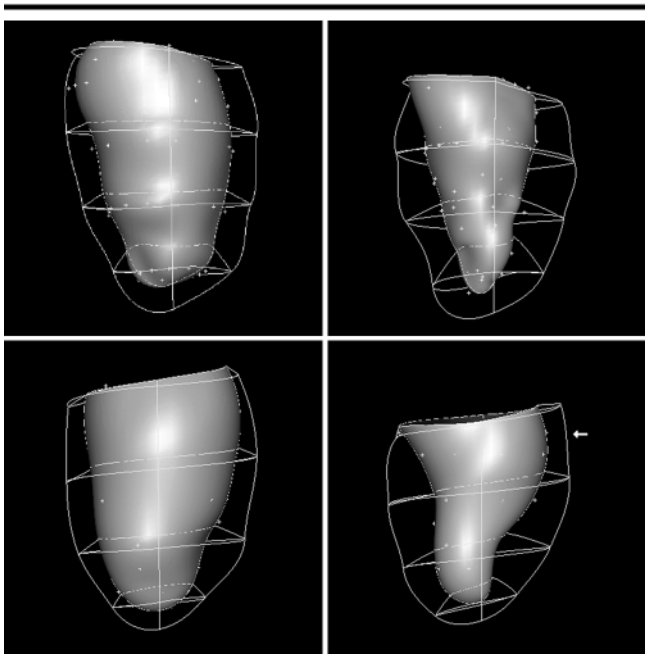

Figure 3. Three-dimensional displays of the model fits in Figure 2. + = endocardial guide points. Endocardial surface is shaded, and element boundaries are drawn as lines. Interventricular septum is to the left. Note the distorted LV shape at ES on the patient image owing to the basal lateral infarct (arrow).

where there was a difference in opinion. Figure 1 shows short-axis sections at ED and ES together with the final boundaries (called "manual contours" in this article since extensive manual correction of the segmentation result was required). The areas outlined in each image were then multiplied by the section thickness plus the section gap and the resultant volumes summed to produce estimates of ED and ES volumes. LV mass was calculated from the mean of the ED and ES myocardial volumes (as the difference between the volumes enclosed by the epicardial and endocardial contours) multiplied by 1.05 g/mL.

Flow quantification.—The phase-contrast velocity images were segmented manually (B.R.C.) into vessel lumen and background. The through-plane velocity component was integrated across the vessel lumen and across all frames in the cycle to produce aortic flow. Note that the flow measurement is insensitive to small inclinations in the angle between the aorta and the section plane (11).

Model Definition

A finite element model was used to represent the geometry of the LV. This model was similar to those used previously to describe LV deformation (14,15). The model consisted of 16 elements, each with cubic interpolation in the circumferential and longitudinal directions. Linear interpolation was used to couple the inner and outer surfaces into a coherent 3D model. The model was defined in a polar coordinate system (Appendix). This simplified the solution process, allowing the radial coordinate (λ) of the model to be fitted as a function of the two angular coordinates (θ and μ in the circumferential and longitudinal directions, respectively). Use of a polar coordinate system imposes two constraints on the shape of the model. First, there must be a straight "central axis" passing within the LV cavity from apex to base. Second, the location of the LV inner and outer surfaces must be uniquely specified on the basis of a radial distance from the central axis at all points. These constraints are not as severe as those typically applied in the case of echocardiography (16), and the piecewise cubic interpolation allows a variety of normal and deformed LV shapes to be accurately modeled, including LV aneurysms and severe hypertrophy (as in reference 14).

Initially, the model was scaled to each heart according to the distance between the base and the apex of the LV. The initial shape of the LV model was a regular ellipsoid, which was obtained by setting the inner and outer surfaces to a constant radial value. The extent of the model in the longitudinal (μ) direction was set to correspond to the most basal extent of the LV in the long-axis images at each time point.

Guide-Point Modeling

Guide points were interactively placed on the images by the user and the two-dimensional image coordinates converted to 3D coordinates with the section position information encoded in the image header. The model shape was fitted to the 3D guide-point positions by minimizing an error function consisting of the sum of a smoothing term and a term penalizing the distance between each guide point and the corresponding model position (Appendix). The smoothing term penalized changes in slope and curvature around the LV, allowing the model to realistically interpolate the very sparse guide-point data. The error function was quadratic in the model parameters, resulting in a simple linear least squares solution process. As the user placed or modified guide points, the model fit was updated in real time. The intersections of the model with the image planes were recalculated after each fit by means of a subdivision algorithm (17) and redisplayed on each image. The user continued to interactively add or modify guide points until the model-image intersections provided a good representation of the boundaries of the LV. Figure 2 shows the intersections of the model with the images shown in Figure 1.

To provide an estimate of interobserver error, guide-point models were created by two operators (A.A.Y., S.F.T.) for each of the volunteers and patients. As previously, papillary muscles were excluded from the myocardium and included in the blood pool.

Model Mass and Volume Comparisons

LV mass and volume could be estimated from the model in a number of ways. To assess the accuracy of the technique, we needed a consistent method of volume calculation that could be used for both manual and guide-point modeling methods; therefore, we used the intersections of the model with each image section plane as model contours at ED and ES (Fig 2). The model contours were then input to the same custom-written software used to calculate the volumes from the manual contours. In this way, the ability of the modeling process to reproduce the manual contours for the purposes of volume calculation could be directly assessed.

TABLE 1
Time Required (Minutes) for Each Study for Estimation of Global Function

Subject	Manual Contouring	Guide-Point Modeling
Patients	41 ± 9	5 ± 3
Volunteers	34 ± 7	7 ± 3

Note.—Data are the means ± SDs.

TABLE 2
Data in Healthy Volunteers (n = 15)

Contour Method	ED Volume (mL)	ES Volume (mL)	LV Mass (g)	Stroke Volume (mL)	Ejection Fraction (%)
Guide-point model					
Operator 1	144.8 ± 26.6	56.2 ± 10.9	148.9 ± 35.6	88.5 ± 16.5	61.2 ± 2.2
Operator 2	140.7 ± 29.3	52.0 ± 10.6	148.8 ± 35.9	88.7 ± 20.4	62.9 ± 3.5
Manual	140.0 ± 28.1	51.6 ± 10.5	147.6 ± 36.5	88.4 ± 18.6	63.1 ± 2.7
Operator 1 vs manual	4.8 ± 4.4*	4.6 ± 3.3*	1.3 ± 4.8	0.1 ± 5.9	−1.9 ± 2.6*
Operator 2 vs manual	0.7 ± 5.6	0.4 ± 4.3	1.3 ± 5.2	0.3 ± 4.4	−0.2 ± 2.4
Operator 1 vs operator 2	4.1 ± 6.6*	4.2 ± 4.6*	0.1 ± 7.3	−0.1 ± 7.1	−1.7 ± 3.1

Note.—Data are the mean paired differences ± SDs.
* $P < .05$ for difference between estimates.

TABLE 3
Data in MI Patients (n = 13)

Contour Method	ED Volume (mL)	ES Volume (mL)	LV Mass (g)	Stroke Volume (mL)	Ejection Fraction (%)
Guide-point model					
Operator 1	137.8 ± 30.3	64.9 ± 14.5	171.4 ± 40.8	72.9 ± 21.3	52.3 ± 7.8
Operator 2	137.9 ± 32.6	63.8 ± 14.5	171.4 ± 41.5	74.0 ± 22.6	53.1 ± 7.4
Manual	136.3 ± 30.6	62.2 ± 14.8	169.0 ± 40.4	74.1 ± 21.4	53.9 ± 7.7
Operator 1 vs manual	1.5 ± 3.5	2.7 ± 3.7*	2.5 ± 4.6	−1.1 ± 4.3	−1.5 ± 2.6
Operator 2 vs manual	1.6 ± 4.0	1.7 ± 2.6*	2.4 ± 5.3	−0.1 ± 4.7	−0.8 ± 2.1
Operator 1 vs operator 2	−0.1 ± 4.6	1.0 ± 3.9	0.1 ± 6.3	−1.1 ± 4.9	−0.7 ± 2.8

Note.—Data are the mean paired differences ± SDs.
* $P < .05$ for difference between estimates.

Statistical Tests

Volumes and mass were compared between the two methods by means of paired t tests. Differences with a P value of .05 were considered statistically significant.

Results

Figure 2 shows the result of the fitting process on typical short-axis images obtained in a volunteer and a patient at 3 months after myocardial infarction. Figure 3 shows the corresponding 3D LV models and illustrates the ability of the model to describe distorted LV shapes. This patient's infarct was located in the basal lateral LV wall, leading to a wall motion abnormality in this region, which is clearly seen in Figure 3. For the 15 volunteers, a mean 66 guide points (range, 49–81) were needed for each study to fit the original images (approximately six per section). For the 13 patients, a mean 32 guide points (range, 22–51) were needed for each study (approximately three per section). Approximately 6 minutes were required by each operator to generate the guide-point models at ED and ES and estimate LV mass and volumes, ejection fraction, and stroke volume for each study. This represents an improvement of five to 10 times over the times required for manual contouring (Table 1).

Table 2 shows the mean values obtained in the volunteers for ED volume and ES volume, LV mass, stroke volume, and ejection fraction. Results are given for both manual and model contours (two operators), together with the mean paired difference and SD of the differences between the two methods and the two operators. Similarly, Table 3 shows the results for the patient group. Figure 4 shows Bland-Altman plots of the differences between the two measures versus their mean. Taken over both groups (volunteers and patients) and both observers, errors in mass and global function indexes were small in all cases (left ventricular mass, 1.8 g ± 4.9 [mean ± SD]; stroke volume, −0.2 mL ± 4.8; ejection fraction, 1.1% ± 2.5%; ED volume, 2.2 mL ± 4.6; and ES volume, 2.3 mL ± 3.8). Although statistically significant differences exist in some of the functional indexes between model and manual methods and between observers for the modeling method, the magnitude of these differences is small in all cases and unlikely to be clinically important. These differences were likely due to biases in the placement of contours by different observers and to differences in the software used to create the manual contours and the guide-point model contours.

The phase-contrast velocity images of the ascending aorta were obtained at the end of a long imaging protocol, as long as 2 hours after acquisition of the cine short-axis sections used for the manual and modeling calculations. In many subjects, heart rate changed substantially between the two measurements (range for the 15 subjects, −12 to +13 beats per minute). The difference in stroke volume between the flow and section-summation methods was found to be strongly correlated to the change in heart rate between the two images ($P < .001$, r = 0.83). This correlation was linear and was likely due to β-adrenergic effects because of the long imaging time. On the basis of analysis of covariance, or ANCOVA, to correct for heart rate as a covariate, there was no difference between the aortic flow and either the guide-point modeling or manual contouring estimates of stroke volume (manual vs phase contrast, 0.6 mL ± 5.4; operator 1 model vs phase contrast, 0.2 mL ± 9.0; operator 2 model vs phase contrast, 0.9 mL ± 7.7). Figure 5 part *A* shows Bland-Altman plots for these comparisons.

Postmortem mass measurements also agreed well with model estimates of LV mass in the eight dogs studied (−0.3 g ± 5.8 [Fig 5 part *B*]).

Discussion

The guide-point modeling method can be used with any mathematic model and 3D image data set (eg, 3D ultrasonography or CT). Use of smoothing constraints in conjunction with guide points provided an intuitive and efficient user interface with which to manipulate the model. Since the position of the guide points influenced the model shape in a consistent 3D manner, relatively few guide points were required for adequate fits to the images (three to six

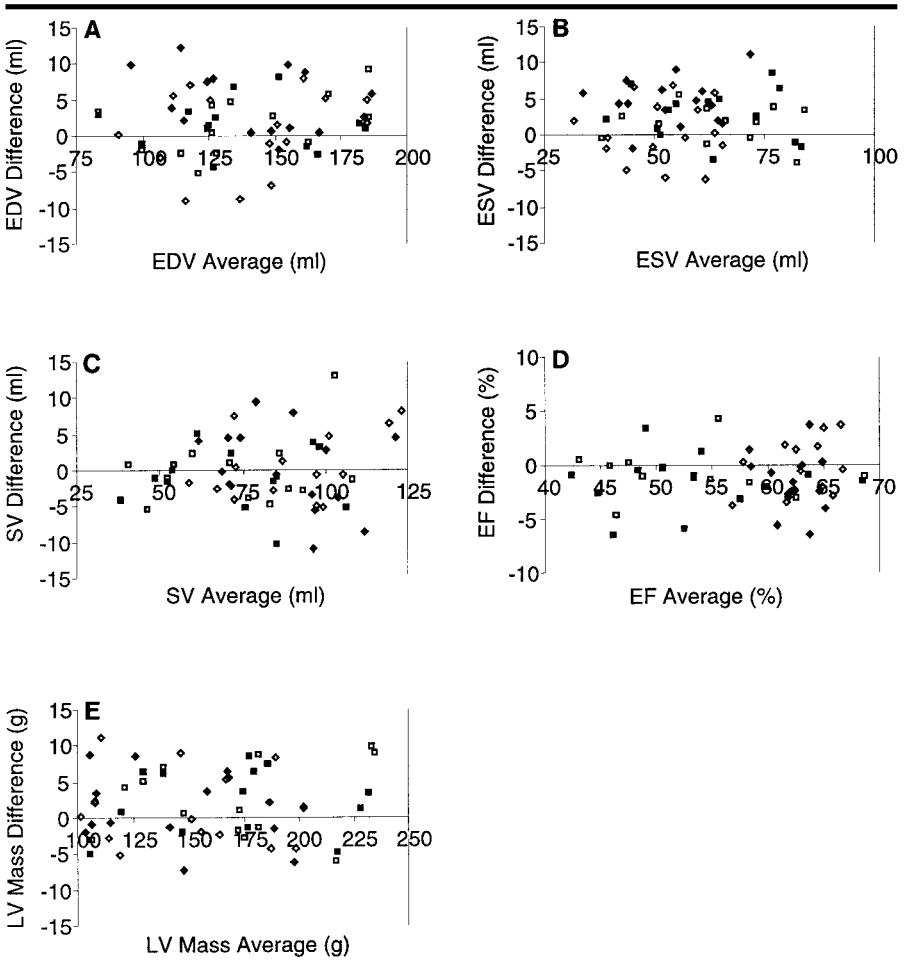

Figure 4. Bland-Altman plots show differences in global function parameters (model minus manual) versus the mean of the two methods. *A*, ED volume (*EDV*); *B*, ES volume (*ESV*); *C*, stroke volume (*SV*); *D*, ejection fraction (*EF*); and *E*, LV mass. ◆ and ◇ = volunteers, ■ and □ = patients; ◆ and ■ = observer 1, ◇ and □ = observer 2.

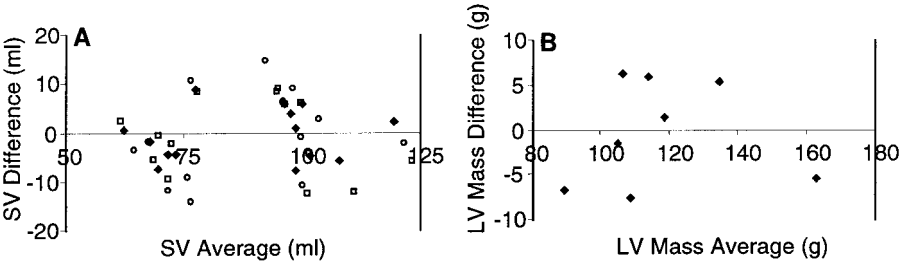

Figure 5. *A*, Bland-Altman plot shows differences in stroke volume (*SV*) between phase-contrast flow measurements (corrected for heart rate) and manual method (◆) and modeling method (□ = observer 1, ○ = observer 2) in volunteers. *B*, Bland-Altman plot shows differences in mass between postmortem measurements and modeling method (single observer) in eight dogs.

points per section), which reduced the amount of user interaction required. In our experiments, more guide points were needed for the volunteers than for the patients with wall motion abnormalities. The breath-hold volunteer images were of much higher quality than were the non–breath-hold patient images, with minimal motion artifact, better signal-to-noise ratio and greater contrast between blood and muscle, particularly about the papillary muscles and endocardial trabeculae. This higher quality may have contributed to the increased number of guide points required for good correspondence between the model and the image in these cases.

The guide-point modeling method relies on the user to successively refine placement of the model on the images. No image processing is required. Current methods that rely on image processing lack the robustness and accuracy necessary for successful clinical application; however, local image information can be included in the model optimization (18).

LV absolute volumes tended to be overestimated with the model contours of operator 1 relative to operator 2 and the manual contours in the healthy group. These differences were spread evenly over all sections and could be equated with a small bias in the perceived position of the boundary. It is vital in any institution that a consensus be achieved among all operators in the placement of ventricular boundaries on the images. Small biases in contour placement can easily lead to large errors in volumes and mass. In this study, the SDs of the differences between manual and modeling methods were small, and the bias is unlikely to be clinically important.

Results of analysis of covariance comparing phase-contrast aortic flow measurements with manual and model estimates of stroke volume showed that there was no effect (other than heart rate) due to the measurement method. The comparison of LV mass with postmortem measurements showed an apparent overestimation of mass with the guide-point method, since papillary muscles were included in the postmortem weighing but were excluded from the guide-point model. The eight dogs were studied after 5–6 months of mitral regurgitation caused by rupture of the chordae and thus exhibited severe LV remodeling due to chronic volume overload (13). The contribution of the papillary muscles to LV mass was therefore likely to be smaller than usual, and some papillary muscle may have been included in the guide-point model owing to failure to distinguish it from LV wall. Also, errors due to trabeculation of the inner surface of the LV, possible inclusion of epicardial fat (together with the specific gravity factor of 1.05 g/mL used for comparison), and the slight overestimation of model mass relative to manual contours (Tables 2, 3) may have combined to produce the apparent overestimation.

The guide-point modeling method was found to reduce the time required to estimate LV mass, ED volume, ES volume, stroke volume, and ejection fraction by a factor of 5–10 without loss of accuracy. In conjunction with recent advances in fast cardiac imaging (3,4), a comprehensive cardiac examination including imaging (scout images plus eight to 12 cine sections in short- and long-axis orientations) and analysis (global and possibly regional function) would typically require less than half an hour to complete. This time saving enables high-spatial-resolution multiplanar MR studies of cardiac function to be efficiently used in routine clinical practice.

Appendix

A finite element model was constructed as described previously (14,15,19). Within each element, the geometry of the LV was given by a weighted mean of values at the nodes:

$$\lambda(\xi_1, \xi_2, \xi_3) = \sum_n \Psi_n(\xi_1, \xi_2, \xi_3)\lambda^n, \quad \text{(A1)}$$

where λ^n are the nodal values, Ψ_n are basis functions that give the relative weighting of each nodal value, and (ξ_1, ξ_2, ξ_3) are the element coordinates. The geometric field λ was defined to be the radial coordinate in a prolate spheroidal coordinate system:

$$\begin{aligned} x &= f\cosh(\lambda)\cos(\mu) \\ y &= f\sinh(\lambda)\sin(\mu)\cos(\theta) \\ z &= f\sinh(\lambda)\sin(\mu)\sin(\theta) \end{aligned} \quad \text{(A2)}$$

where (λ, μ, θ) are the radial, longitudinal, and circumferential coordinates of the polar system and (x, y, z) are the corresponding rectangular cartesian coordinates. The focal length f of the prolate system was chosen so that the $\lambda = 1$ surface gave a good initial approximation of the LV epicardial surface. This provided an overall scale factor for each case. In each element, element coordinates ξ_1, ξ_2, and ξ_3 were in the circumferential, longitudinal, and transmural directions, respectively. The basis functions were chosen to be bicubic Hermite in ξ_1 and ξ_2 and linear in ξ_3 (19). Nodal values were shared between neighboring elements to give continuity in both slope and position throughout the LV. The model consisted of 16 3D elements: four elements in the longitudinal direction by four elements in the circumferential direction (Fig 3).

The model was fitted to guide-point data by minimizing the following error function:

$$E = S(\lambda) + \sum_g [\lambda(\xi_g) - \lambda_g]^2, \quad \text{(A3)}$$

where λ_g are the positions of the guide-point data and $\lambda(\xi_g)$ are the model positions at element coordinates ξ_g corresponding to λ_g. The element coordinates were found by projecting the guide data onto the model along lines of constant μ and θ. $S(\lambda)$ denotes a smoothing term that was included in the error function to constrain the model to smoothly interpolate between the sparse guide points. As done previously (20), we used a weighted Sobolev norm that penalized displacement of the model from a prior shape:

$$\begin{aligned} S(\lambda) = \int_\Omega & \alpha_1\left[\frac{\partial u}{\partial \xi_1}\right]^2 + \alpha_2\left[\frac{\partial u}{\partial \xi_2}\right]^2 \\ & + \beta_1\left[\frac{\partial^2 u}{\partial {\xi_1}^2}\right]^2 + \beta_2\left[\frac{\partial^2 u}{\partial {\xi_2}^2}\right]^2 \\ & + \gamma_1\left[\frac{\partial^2 u}{\partial \xi_1 \partial \xi_2}\right]^2 + \gamma_2\left[\frac{\partial^2 u}{\partial \xi_1 \partial \xi_3}\right]^2 \\ & + \gamma_3\left[\frac{\partial^2 u}{\partial \xi_2 \partial \xi_3}\right]^2 d\Omega, \end{aligned} \quad \text{(A4)}$$

where $u = \lambda - \lambda^*$, where λ^* is the prior shape (in this article, $\lambda^* = 1$ [ie, a regular ellipsoid] is used for the prior shape). The weights α_1 and α_2 penalized the slope of the displacement field in the circumferential and longitudinal directions, respectively, whereas the weights β_1 and β_2 penalized curvature, and the weights γ_1, γ_2, and γ_3 coupled slopes between directions. The smoothing weights used in this article are $\alpha_1 = \alpha_2 = 0$, $\beta_1 = \beta_2 = 0.001$, $\gamma_1 = \gamma_2 = \gamma_3 = 0.01$. The issue of which weights are "optimal" for guide-point fitting remains an active area of research. However, the optimality criterion is difficult to quantify since the user always places the guide points in such a way as to adequately model the ventricle. A wide range of weights were tried in our experiments, and these values provided good results in all cases.

The error function (Eq [A3]) was quadratic in the unknown nodal parameters (λ^n), allowing direct solution by means of the standard least squares methods.

Acknowledgments: We thank Dr Tom Gentles, MBChB, (Department of Paediatrics) and Dr Chris Occleshaw, MBChB, (Department of Radiology) of Green Lane Hospital, Auckland, New Zealand, for their assistance with the recruitment and imaging of the volunteers. We also thank Andrew Cantell, BE, for his technical expertise.

References

1. Reichek N. Magnetic resonance imaging for assessment of myocardial function. Magn Reson Q 1991; 7:255–274.
2. Pattynama PMT, De Roos A, Van der Wall EE, Van Voorthuisen AE. Evaluation of cardiac function with magnetic resonance imaging. Am Heart J 1994; 128:595–607.
3. Atkinson DJ, Edelman RR. Cineangiography of the heart in a single breath hold with a segmented turboFLASH sequence. Radiology 1991; 178:357–360.
4. Foo TKF, Bernstein MA, Aisen AM, Hernandez RJ, Collick BD, Bernstein T. Improved ejection fraction and flow velocity estimates with use of view sharing and uniform repetition time excitation with fast cardiac techniques. Radiology 1995; 195:471–478.
5. Germain P, Roul G, Kastler B, Mossard JM, Bareiss, Sacrez A. Inter-study variability in left ventricular mass measurement: comparison between M-mode echocardiography and MRI. Eur Heart J 1992; 13:1011–1019.
6. Pattynama PMT, Lamb HJ, van der Velde EA, van der Wall EE, de Roos A. Left ventricular measurements with cine and spin-echo MR imaging: a study of reproducibility with variance component analysis. Radiology 1993; 187:261–268.
7. Bottini PB, Carr AA, Prisant LM, Flickinger FW, Allison JD, Gottdiener JS. Magnetic resonance imaging compared to echocardiography to assess left ventricular mass in the hypertensive patient. Am J Hypertens 1995; 8:221–228.
8. Staib LH, Duncan JS. Boundary finding with parametrically deformable models. IEEE Trans Pattern Anal Machine Intelligence 1992; 14:1061–1075.
9. Thedens DR, Skorton DJ, Fleagle SR. Methods of graph searching for border detection in image sequences with applications to cardiac magnetic resonance imaging. IEEE Trans Med Imaging 1995; 14:42–55.
10. Singleton HR, Pohost GM. Automatic cardiac MR segmentation using edge detection by tissue classification in pixel neighborhoods. Magn Reson Med 1997; 37:418–424.
11. Pelc NJ, Herfkens RJ, Shimakawa A, Enzmann DR. Phase contrast cine magnetic resonance imaging. Magn Reson Q 1991; 7:229–254.
12. Johnson DB, Foster RE, Barilla F, et al. Angiotensin-converting enzyme inhibitor therapy affects left ventricular mass in patients with ejection fraction >40% after acute myocardial infarction. J Am Coll Cardiol 1997; 29: 49–54.
13. Young AA, Orr R, Smaill BH, Dell'Italia LJ. Three-dimensional changes in left and right ventricular geometry in chronic mitral regurgitation. Am J Physiol 1996; 271: H2689–H2700.
14. Young AA, Kramer CM, Ferrari VA, Axel L, Reichek N. Three-dimensional left ventricular deformation in hypertrophic cardiomyopathy. Circulation 1994; 90:854–867.
15. Young AA, Kraitchman DL, Dougherty L, Axel L. Tracking and finite element analysis of stripe deformation in magnetic resonance tagging. IEEE Trans Med Imaging 1995; 14: 413–421.
16. Schiller NB, Shah PM, Crawford M, et al. Recommendations for quantitation of the left ventricle by two-dimensional echocardiography. J Am Soc Echocardiogr 1989; 2:358–367.
17. Lorensen WE, Cline HE. Marching cubes: a high resolution 3D surface construction algorithm. Comput Graph 1987; 21:163–169.
18. McInerney T, Terzopoulos D. Deformable models in medical image analysis: a survey. Med Image Analysis 1996; 1:91–108.
19. Nielsen PMF, Le Grice IJ, Smaill BH, Hunter PJ. Mathematical model of the geometry and fibrous structure of the heart. Am J Physiol 1991; 260:H1365–H1378.
20. Terzopoulos D. Regularization of inverse problems involving discontinuities. IEEE Trans Pattern Anal Machine Intelligence 1986; 8:413–424.